The VN3H defect in diamond: A quantum-mechanical characterization

The VN_3H Defect in Diamond: A Quantum-Mechanical Characterization

Francesco Gentile,[1] Simone Salustro,[1] Mauro Causà,[2] Alessandro Erba,[1] Philippe Carbonniére,[3] and Roberto Dovesi[1]

[1)] *Dipartimento di Chimica, Università di Torino and NIS (Nanostructured Interfaces and Surfaces) Centre, Via P. Giuria 5, 10125 Torino, Italy*

[2)] *Dipartimento di Ingengeria Chimica, dei Materiali e delle Produzioni Industriali DICMAPI, Università degli Studi di Napoli Federico II, Piazzale Vincenzo Tecchio 80, 80125, Napoli, Italy*

[3)] *Equipe de Chimie Physique, IPREM UMR5254, Université de Pau et des Pays de l'Adour, 64000 Pau (France)*

(Dated: 12 June 2017)

The VN_3H defect in diamond (a vacancy surrounded by three nitrogen and one carbon atoms, the latter being saturated by a hydrogen atom) is investigated quantum-mechanically by use of a periodic supercell approach, an all-electron Gaussian-type basis set, "hybrid" functionals of the density-functional-theory, and the CRYSTAL program. Three fully-optimized structural models (supercells containing 32, 64 and 128 atoms) are considered to investigate the effect of defect concentration. The electronic configuration of the defect is reported along with a description of its structural features. In particular, the influence of the lone-pair electrons of the three nitrogen atoms on the C-H bond is discussed. A thorough characterization of the vibrational spectroscopic features of the VN_3H defect is also presented, where the anharmonicity of the most relevant normal modes is discussed. The infrared and Raman spectra show specific peaks, which allow for the identification of this particular defect among the many defects that are commonly present in both natural and irradiation-damaged diamonds. In particular, the main feature of the spectral fingerprint of the defect (i.e. the C-H stretching mode), experimentally observed at 3107 cm^{-1}, is here computed at 3094 cm^{-1} with the B3LYP "hybrid" functional (with an anharmonic redshift of 157 cm^{-1} with respect to its harmonic value). The role played by the three nitrogen atoms on the spectral features of the defect is clearly identified through the redshift due to the $^{14}N \rightarrow {}^{15}N$ isotopic substitution.

Keywords: hydrogen in diamond, vacancy, point-defects, supercell, vibrational spectroscopy, anharmonicity

I. INTRODUCTION

Nitrogen and hydrogen atoms are among the most common impurities in diamond. In particular, hydrogen atoms are included either during the growth of natural diamonds or via chemical-vapor-deposition (CVD) processes. While certainly present at the surfaces, they are also thought to be incorporated in the bulk, where they can form several defects in combination with vacancies and nitrogen aggregates.[1,2]

Vibrational spectroscopies, such as infrared (IR) and Raman, are among the best techniques for the characterization of point-defects in diamond. The properties of hydrogen atoms in bulk diamond, including vibrational spectroscopic aspects, have been discussed in two comprehensive reviews in 2002 and 2007.[3,4] The former focuses on the theoretical/computational description of a set of hydrogen-containing defects, while the latter provides an experimental overview. Not all of the bulk hydrogen atoms in diamond are expected to produce some IR-active vibration modes, but some of them certainly do through stretching and bending modes. In this respect, one of the first attributions to hydrogen atoms of a set of peaks in the 1405-4495 cm^{-1} range of the infrared spectrum of diamond was reported in 1959 by Charette.[5] In particular, the sharp vibrational peaks at 3107 and 1405 cm^{-1} that appear in almost all types of natural diamonds have been attributed to hydrogen atoms,[1,6–8] that are considered to be strongly bonded to a carbon atom, with weak perturbations due to neighboring nitrogen atoms.[3,4,9]

From a computational perspective, Briddon and coworkers have performed some of the most systematic and careful studies of defects in diamond.[3,10–12] In particular, a couple of recent studies report about the *ab initio* simulation of the VN_3H defect, and propose the attribution of the 3107 cm^{-1} peak to this defect.[11,12] Calculations were performed by using both LDA and GGA functionals of the density-functional-theory (DFT), and a Gaussian-type basis set with pseudopotentials. IR intensities were computed numerically by estimating the variation of the dipole moment of a large cluster ($C_{293}H_{172}$) that mimics the bulk situation. The resulting harmonic frequencies for the stretching and bending modes were computed at 3037 and 1361 cm^{-1} for LDA and 3125 and 1366 cm^{-1} for GGA.

In the present study, we perform a quantum-mechanical characterization of structural, electronic, energetic and vibrational spectroscopic features of the VN_3H defect, with some methodological improvements with respect to previous descriptions. Calculations are performed with hybrid functionals of the DFT, which, owing to their fraction of exact non-local exchange, correct to a large extent for the self-interaction error typical of pure DFT functionals,[13] and are thus expected to provide a more reliable description of many features

of the system,[14–18] particularly so when hydrogen atoms are involved. A second improvement is related to the explicit anharmonic treatment of the C-H stretching and bending modes. For instance, with respect to the purely harmonic value, anharmonicity is here documented to redshift by 157 cm^{-1} the vibration frequency of the stretching mode, which makes such an explicit anharmonic treatment mandatory for a quantitative comparison with experimental data. A third improvement is represented by the fact that IR and Raman intensities are computed consistently on the same periodic system used to obtain the vibrational frequencies, and are evaluated analytically, through a Coupled-Perturbed-Hartree-Fock/Kohn-Sham (CPHF/KS) scheme,[19–22] as already done in our recent studies of vibration properties of other defects in diamond.[23–27] Finally, graphical animations of all vibration modes have been produced, which allow for an effective analysis of the contributions of individual atoms or groups of atoms to the vibration modes.[28]

The paper is structured as follows: methodological and computational aspects are discussed in Section II; a structural, electronic and vibrational spectroscopic characterization of the VN_3H defect in diamond is reported and discussed in Section III; conclusions are drawn in Section IV.

II. COMPUTATIONAL MODELS AND DETAILS

All calculations are performed with a developmental version of the CRYSTAL14 program.[29] Use is made of the B3LYP global hybrid functional.[30,31] An all-electron basis set of Gaussian-type functions is adopted (Pople's 6-21G) for C and N atoms, the exponent of the most diffuse *sp* shell being 0.23 and 0.30 $bohr^{-2}$ for C and N, respectively. For hydrogen, a 6-31G basis set is used.[32] The defect formation energy is also calculated with larger basis sets (6-21G*, 6-31G and 6-31G*) and other functionals: LDA,[33] PBE,[34] the global-hybrid PBE0,[35], and the range-separated hybrid HSE06.[36]

The truncation of the Coulomb and exchange infinite lattice series is controlled by five thresholds T_i, as discussed in the CRYSTAL manual,[37] which are here set to 8 (T_1-T_4) and 16 (T_5). The convergence threshold on energy for the self-consistent-field (SCF) procedure is set to 10^{-8} Hartree for structural optimizations and to 10^{-10} Hartree for vibration frequency calculations.

The DFT exchange-correlation contribution to the Fock matrix is evaluated by numerical integration over the unit cell volume. Radial and angular points for the integration grid are generated through Gauss-Legendre radial quadrature and Lebedev two-dimensional angular point distributions. The default pruned grid with 75 radial and 974 angular points is used, whose accuracy can be measured by comparing the integrated charge density in the largest supercell here considered (128 atoms): 766.010 $|e|$, with the total number of 766 electrons in the unit cell.

A periodic supercell approach is used to simulate different defect concentrations. Supercells containing 32, 64 and 128 atoms are considered (to be referred to in the following as S_n, with n=32, 64 or 128). Reciprocal space is sampled using a regular sub-lattice, centered at the origin (Γ-point) with a shrinking factor of 8 for S_{32} and S_{64}, and of 4 for S_{128}, which correspond to a sampling over 65 (S_{32} and S_{64}) and 13 (S_{128}) $\mathbf{k}$-points in the irreducible part of the Brillouin zone.

A. Harmonic Frequencies and the IR and Raman Spectra

Vibration frequencies at the Γ point are obtained within the harmonic approximation by diagonalizing the mass-weighted Hessian matrix W, whose elements are defined as:[38–42]

$$W^{\Gamma}_{\alpha i,\beta j} = \frac{H^{\mathbf{0}}_{\alpha i,\beta j}}{\sqrt{M_\alpha M_\beta}} \quad \text{with} \quad H^{\mathbf{0}}_{\alpha i,\beta j} = \left(\frac{\partial^2 E}{\partial u^{\mathbf{0}}_{\alpha i} \partial u^{\mathbf{0}}_{\beta j}} \right) , \tag{1}$$

where M_α and M_β are atomic masses and the elements $H^{\mathbf{0}}_{\alpha i,\beta j}$ of the Hessian matrix are second energy derivatives with respect to pairs of Cartesian atomic displacements within the reference cell. Frequency shifts due to isotopic substitutions can be calculated *a posteriori*, at no computational cost, simply by changing the masses in Eq. (1). The elements of the Hessian matrix are computed as numerical finite-differences of analytical gradients, either with a one-sided or a two-sided formula. Previous calculations have shown that for most bulk systems without hydrogen atoms a one-sided finite-difference formula provides fairly stable results, with differences on the frequencies often smaller than 1 cm^{-1} with respect to a two-sided one.[38,43,44] The presence of hydrogen atoms implies a large anharmonicity and thus requires special care (see Section II B below).

Integrated intensities for IR absorption $\mathcal{I}_p$ are computed for each vibration mode p by means of the mass-weighted effective-mode Born-charge vector $\mathbf{Z}_p$,[45,46] as evaluated through an analytical CPHF/KS approach:[19,20]

$$\mathcal{I}_p \propto \left| \mathbf{Z}_p \right|^2 . \tag{2}$$

Raman intensities are also computed analytically through a second-order CPHF/KS approach.[21,22]

B. Anharmonic Treatment of C-H Stretching and Bending Modes

The strongly anharmonic nature of vibration modes involving hydrogen atoms is well-known both in a molecular and in a solid state context.[47–53] In this respect, the drawbacks of a purely-harmonic description of atomic vibrations are: i) the assumption of a quadratic behavior

for the potential-energy surface (PES), and ii) the independence of the normal modes of vibration. Both limitations can be overcome by means of an explicit anharmonic treatment where i) higher-order terms in the expansion of the PES are included, and ii) couplings among normal modes are taken into account. The PES can indeed be expanded in a Taylor series with respect to the m harmonic normal modes as:

$$V(Q_1, Q_2, \ldots, Q_m) = \sum_i \frac{\omega_i^2}{2} Q_i^2 + \frac{1}{3!} \sum_{i,j,k} \eta_{ijk} Q_i Q_j Q_k + \\ + \frac{1}{4!} \sum_{i,j,k,l} \eta_{ijkl} Q_i Q_j Q_k Q_l + \cdots ; \quad (3)$$

where Q_i is the i-th harmonic normal coordinate, ω_i the corresponding harmonic frequency, and where η_{ijk} and η_{ijkl} are third- and fourth-energy derivatives with respect to normal coordinates, respectively.

In a developmental version of the CRYSTAL program, algorithms have been implemented to numerically evaluate (as finite differences of analytical gradients) all cubic and one-, two- and three-mode quartic terms in the expansion of the PES, as proposed by Lin *et al.* in their energy-gradient-Hessian (EGH) scheme.[54] In this study, one- and two-mode cubic as well as one- and two-mode quartic terms are computed by means of a five-point finite difference formula where the energy and gradients are evaluated along each normal coordinate from -0.7 to 0.7 in units of the "classical amplitude" of each harmonic oscillator.

Two methods are used to compute the anharmonic correction to the fundamental vibrational transitions, as implemented in a developmental version of the CRYSTAL program: the vibrational self-consistent-field (VSCF) method, where each mode vibrates in the average potential generated by all other modes,[55–58] and the vibrational configuration interaction (VCI) method, which takes into explicit account the correlation among modes.[59–61] In the VCI calculation, the configurational space is limited in such a way to include all and only those configurations with up to 9 simultaneous excitations.

The two degenerate modes describing the C-H bending (b) and the mode describing the C-H stretching (s) are here explicitly considered, where it is found (see discussion in Section III) that while the anharmonicity of the stretching mode is mostly due to higher-order diagonal terms in the PES (η_{sss} and η_{ssss}), the anharmonicity of the bending is dominated by the coupling with the stretching (through mixed energy derivatives in the PES such as η_{bss}, η_{bbs}, η_{bsss}, η_{bbss}, η_{bbbs}).

III. RESULTS AND DISCUSSION

A. Structural, Electronic and Energetic Features

The structure and charge distribution of the VN_3H defect in diamond, as obtained after full structural relaxation at B3LYP level for the largest S_{128} supercell here considered, are given in Figure 1. Among other structural features, the description of the C-H bond turns out to be of particular interest for this system given that, as we will discuss in Section III B below, the corresponding normal modes of vibration do constitute the spectral fingerprint of the VN_3H defect. In order to quantitatively evaluate the influence of the three N atoms on the C-H bond, the isobutane molecule has also been investigated, in the same computational conditions as the bulk system, to describe the local features of the C-H bond without the strong polarization induced by the presence in the bulk of the lone-pair electrons of the three nitrogen atoms on the opposite side of the vacancy hole.

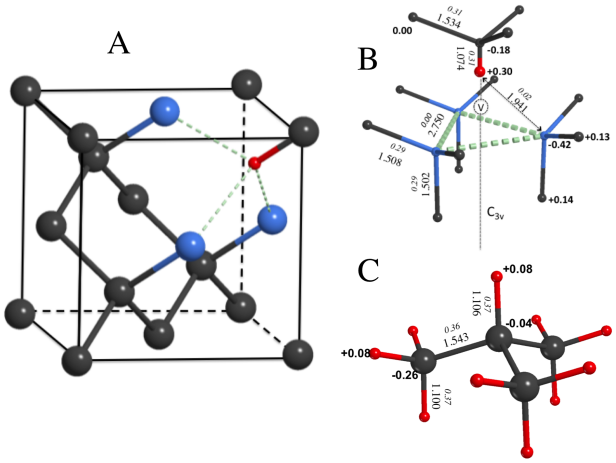

FIG. 1. (A) A graphical representation of the optimized structure of the VN_3H defect in diamond, which belongs to the C_{3v} point-symmetry (carbon atoms in gray, nitrogen atoms in blue and the hydrogen atom in red). (B) The local region around the defect is shown where bond lengths (in Å, large), atomic Mulliken charges (in $|e|$, in bold) and bond populations (in $|e|$, in italic) are reported, as computed on the largest S_{128} supercell at B3LYP level. (C) Same as in panel B for the isobutane molecule.

In the bulk, the C-H bond points towards the center of the triangle formed by the three nitrogen atoms; as a consequence, the C-H bond length in the bulk, 1.074 Å, is shorter by 0.03 Å than in the molecule (see panel C of Figure 1). Another consequence of the repulsion from the N lone-pair electrons is the rather strong charge polarization of the C-H bond. The Mulliken net charges are indeed 0.30 $|e|$ on H and -0.18 $|e|$ on C, with a C-H bond population of 0.31 $|e|$. For comparison, in isobutane the corresponding net charges are much smaller (0.08 $|e|$ on H and -0.04 $|e|$ on C), and the bond population is higher, 0.37 $|e|$. To summarize, due to the presence of the three neighboring N atoms, the C-H bond turns out to be shorter, more ionic (higher net atomic charges) and correspondingly less covalent (smaller bond population) in the bulk than in the molecule.

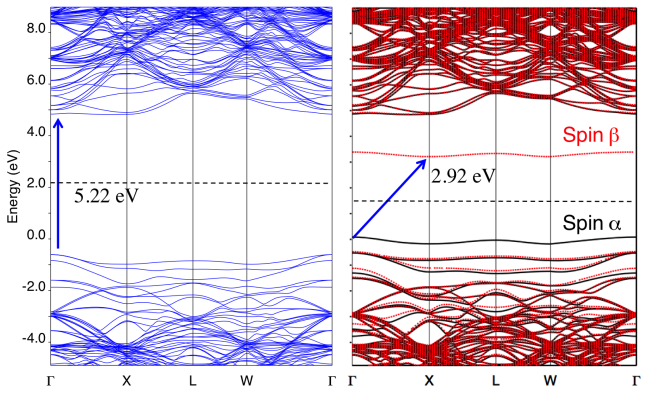

FIG. 2. Electronic band structure of the unsaturated VN_3 (right panel) and of the H-saturated VN_3H (left panel) defect in diamond. While VN_3H is a closed-shell system, VN_3 is open-shell and black and red bands correspond to α and β electrons, respectively. Both panels refer to the S_{128} supercell. The dashed black line is the Fermi level.

As regards the nitrogen atoms, their net charge is -0.42 $|e|$; it is +0.14 $|e|$ on each of the three carbon atoms linked to them with a N-C bond length of 1.50 Å, so that the defect region (up to second neighbors from the vacancy) is essentially neutral. Indeed, the next C-C bond length is already about the same as in pristine diamond, 1.56 Å. This very local structural and electrostatic nature of the VN_3H defect in diamond is expected to significantly affect the C-H stretching and bending modes.

The band structure of the VN_3H defect in diamond, as computed at the B3LYP level, is reported in Figure 2 (left panel), where it is compared with that of the unsaturated VN_3 center (i.e. the defect with 3 nitrogen atoms and one carbon atom around the vacancy, with no H). The main difference between the two systems is that while the former is closed-shell, the latter is an open-shell system with an unsaturated carbon atom. In the VN_3 system, the two bands within the gap correspond to the unpaired electron on the unsaturated C atom: the lowest one is occupied (spin up), and is 0.62 eV above the valence bands, whereas the highest (spin down) is unoccupied, the energy difference between the two being 2.92 eV. The two degenerate bands of E symmetry just below the occupied (spin up) band host the nitrogen lone-pair electrons (the third one, of A_1 symmetry, being much lower in energy, at about -5 eV). Upon saturation with hydrogen (left panel), the spin up occupied band is strongly stabilized and is found below the two degenerate lone-pair bands of E symmetry.

As a further characterization of the defect, we calculate the homolytic C-H bond cleavage, where the H atom is dissociated to give the VN_3 radical system. The corresponding dissociation energy E_H is defined as:

$$E_H = E_{VN_3} + \frac{1}{2}E_{H_2} - E_{VN_3H}\,. \qquad (4)$$

TABLE I. C-H homolytic cleavage energy E_H and defect formation energy E_f (in eV) for the VN_3H defect in diamond, as computed with different functionals of the DFT and according to Eqs. (4) and (5). The values (in hartree, E_h) of all the energy terms entering the definition of these two quantities are also reported. All values correspond to the S_{64} supercell.

Method	E_{H_2} (E_h)	E_{N_2} (E_h)	E_C (E_h)	E_{VN_3H} (E_h)	E_{VN_3} (E_h)	E_H (eV)	E_f (eV)
B3LYP	-1.1687	-109.3126	-2435.5789	-2447.8273	-2447.1811	1.7	2.2
PBE0	-1.1639	-109.2405	-2434.8068	-2447.0175	-2446.3683	1.8	1.5
HSE06	-1.1636	-109.2394	-2434.7622	-2446.9741	-2446.3254	1.8	1.5
PBE	-1.1620	-109.2490	-2434.4882	-2446.7257	-2446.0812	1.7	1.7
LDA	-1.1332	-108.4756	-2416.0004	-2428.3025	-2427.6565	2.2	-0.6

The E_H values, and all the other energies involved in Eq. (4) are given in Table I as computed with the S_{64} supercell and with 5 different functionals of the DFT, belonging to different classes: a local density LDA, a generalized-gradient GGA, two global hybrids B3LYP and PBE0 and a range-separated hybrid HSE06. The process is found to be endothermic with all functionals by about 1.7-1.8 eV, with a larger value of 2.2 eV with LDA. It is interesting to compare these values with the homolytic dissociation energy of similar reactions on simple molecules (see Table S1 in Supplementary Material, where the same computational set-up has been used). For ternary carbon atoms (a carbon linked to one H and three C atoms, as in isobutane), E_H is found to be 2.1 eV, just 0.3 eV higher than for VN_3H, which further confirms the strong localization of the electronic features in the VN_3H defect. For secondary carbon atoms, it increases by about 0.2 eV, and a similar change is observed when going from secondary to primary carbon atoms. Table I also reports the defect formation energy E_f, as evaluated according to the equation:

$$E_f = E_{VN_3H} - \left(nE_C + \frac{3}{2}N_2 + \frac{1}{2}E_{H_2}\right)\,; \qquad (5)$$

where n is the number of carbon atoms in the supercell, E_C is the energy of a C atom in pristine diamond, and the other two contributions refer to the H_2 and N_2 molecules. Also in this case the process is strongly endothermic, as reactants (diamond and molecules) are very stable quantities and entropic terms are not accounted for.

B. IR and Raman Spectroscopic Features

As anticipated in the Introduction, many defects in diamond have rather specific vibrational spectroscopic fingerprints that, once fully-characterized, can allow for their identification. In this respect, it is useful to remind

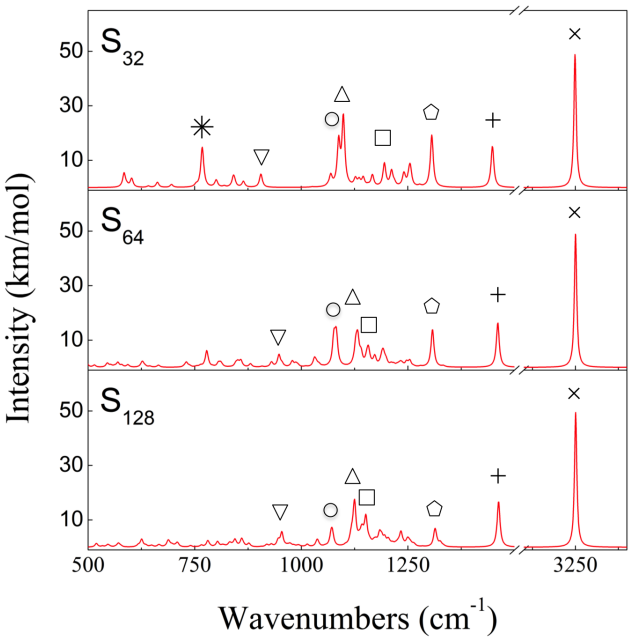

FIG. 3. The simulated IR spectrum of the VN_3H defect in diamond at three defect concentrations (corresponding to S_{32}, S_{64} and S_{128} super-cells) is reported as computed at B3LYP level. A Lorentzian function with a width of 8 cm^{-1} has been used for each computed peak to generate the spectrum.

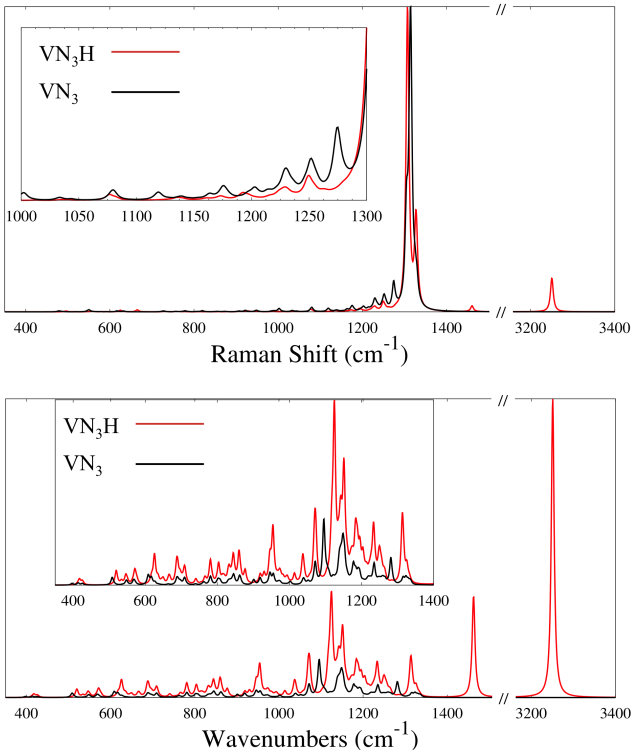

FIG. 4. Comparison between computed Raman (upper panel) and IR (lower panel) spectra for the VN_3H defect (red lines) and for the VN_3 defect (black lines) on the largest S_{128} supercell at the B3LYP level.

that the IR and Raman spectra of pristine diamond are fairly simple as in the former there are no allowed transitions and the latter is characterized by a single intense peak at 1332 cm^{-1}. With our computational setup the position of this peak is found at 1317 cm^{-1} as computed with the B3LYP functional. It follows that all the additional features that appear in the experimental IR and Raman spectra arise from the presence of defects.

The IR harmonic vibrational spectrum, as computed at three defect concentrations corresponding to the S_{32}, S_{64}, and S_{128} supercells, is shown in Figure 3. As a general remark, we note that the high-wavenumber peaks, which correspond to very localized nuclear vibrations in the defect region, are found to be almost independent of defect concentration. This is clearly the case for the C-H stretching (3249, 3250 and 3251 cm^{-1} for S_{32}, S_{64}, and S_{128}, respectively), the C-H bending (1448, 1461 and 1463 cm^{-1}), and other four peaks marked by open circles, up-pointing triangles, squares and pentagons in the figure (whose largest shift is of just 9 cm^{-1}). On the contrary, the peaks at lower wave-numbers clearly refer to more collective vibration modes and vary much more significantly with the defect concentration, as is the case of the peak at about 780 cm^{-1} in S_{32} (marked with an asterisk), whose intensity is very much damped for smaller concentrations, or the peak at about 900 cm^{-1} in S_{32} (open down-pointing triangle), which shifts by about 50 cm^{-1}.

In the VN_3H defect, the Raman active modes coincide with the IR-active ones. The corresponding intensities, however, are quite different, so that the overall structure of the two spectra looks quite different. The computed Raman spectrum, reported in the upper panel of Figure 4, is dominated by the very intense band at about 1310 cm^{-1}, resulting from the superposition of four peaks: one at 1307 cm^{-1} of E symmetry and with an arbitrary intensity of 1000, one at 1308 cm^{-1} of A_1 symmetry with an intensity of 459, one at 1327 cm^{-1} of E symmetry and an intensity of 287, and finally one at 1329 cm^{-1} of A_1 symmetry, whose intensity is 163. This band clearly corresponds to the splitting of the only peak of pristine diamond due to symmetry-breaking. Two peaks appear above this value in the spectrum that are directly related to the defect: the C-H stretching at 3251 cm^{-1} and the C-H bending at 1463 cm^{-1}. Let us note that the intensities of these defect-specific spectral features (159 and 27 in arbitrary units) are much smaller that that of the main band at about 1310 cm^{-1} and thus they might not be easily detectable in the experiment, unless explicitly looked for.

In Figure 4, a comparison is also presented of the Raman (upper panel) and IR (lower panel) spectra of the VN_3H defect with those of the corresponding unsaturated radical system VN_3. As one might expect, the VN_3 spectra are much less structured than those of VN_3H. In par-

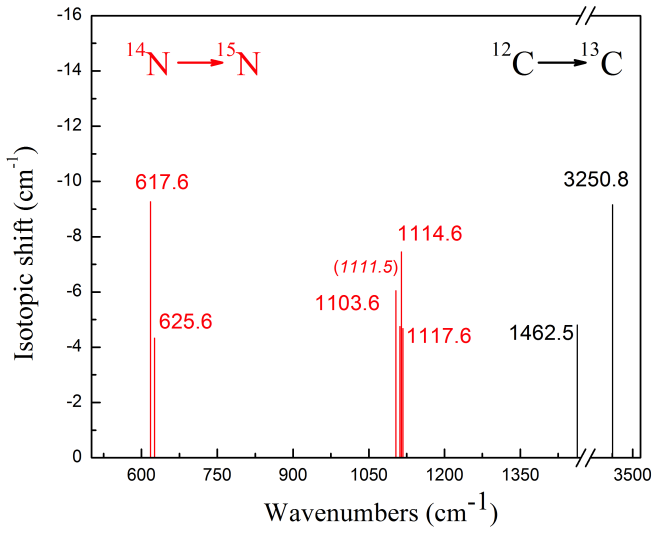

FIG. 5. Computed shifts of peak positions due to isotopic substitution. Both the ^{14}N→ ^{15}N substitution of the three N atoms (red lines) and the ^{12}C → ^{13}C substitution for the C atom of the C-H bond (black lines) are investigated for the largest S_{128} supercell. The intensity of the mode within parentheses is null.

ticular, all peaks above 1300 cm^{-1} disappear as they are almost entirely localized on the hydrogen atom in VN_3H. Interestingly, the Raman spectrum of the VN_3 system shows three sharp shoulder peaks at 1230, 1251 and 1274 cm^{-1} that are not very pronounced in the VN_3H spectrum.

In order to investigate which is the role played by the three nitrogen atoms on the spectral fingerprint of the defect, we have performed the ^{14}N → ^{15}N isotopic substitution. The vibration modes that mostly involve N atoms are found to be very localized in two narrow spectral regions: 618-626 cm^{-1} and 1104-1118 cm^{-1}. The shifts in peak positions due to isotopic substitution are given in Figure 5. Graphical animations of the vibration modes confirm the large contribution of N atoms to those modes.[28] In particular, the modes in the 618-626 cm^{-1} region can be understood as bending motions, whereas those in the 1104-1118 cm^{-1} region as stretching motions. The right hand side of Figure 5 reports the isotopic shifts of those peaks where the C atom of the C-H bond is strongly involved, upon ^{12}C → ^{13}C isotopic substitution. As expected,[62] the C-H stretching mode shifts by 9 cm^{-1} while the bending by about 5 cm^{-1}. Finally, the H → D substitution generates a shift of 854 and 437 cm^{-1} for the stretching and bending modes, respectively.

Overall, the two intense peaks in the IR spectrum at 3107 and 1405 cm^{-1} represent the clearest evidence of the presence of a hydrogen atom linked to a carbon atom that is a first-neighbor of a vacancy in diamond. The accurate description of these modes is thus crucial in order to reliably characterize the spectroscopic fingerprint of the VN_3H defect. As it is well-known, the nuclear vibrations involving H atoms are strongly anharmonic (particularly so for the stretching modes), which makes a purely-harmonic computational description of those modes not accurate enough for a quantitative characterization. As regards the specific case of the C-H modes, anharmonicity is estimated to red-shift the harmonic stretching frequency by about 120-140 cm^{-1} and the bending frequency by about 10-40 cm^{-1} for many organic molecules.[63–67]

In order to evaluate the anharmonicity of the C-H stretching and bending modes, we have performed VSCF and VCI calculations with the B3LYP functional on the S_{64} supercell. Before discussing our results, let us recall that the main implications of the harmonic approximation are: i) the truncation to second-order of the Taylor expansion of the PES in Eq. (3), and ii) the corresponding independence of normal modes of vibration. The so-called *intrinsic* anharmonicity of a mode can be evaluated by retaining the second assumption (i.e. by neglecting couplings among modes) but at the same time by taking into account higher-order terms in the PES (such as cubic, quartic, etc.) for the considered mode: only diagonal terms of the type η_{iii}, η_{iiii}, etc. would be included in the PES expansion. A *complete* anharmonic description implies the evaluation of all terms in the PES expansion, that is to say that both higher-order diagonal and mixed terms of the type η_{iij}, η_{iijj}, etc. would be considered. In the present calculations, the PES is described in such a way to include cubic and quartic terms involving only the three modes proper of the C-H fragment: two degenerate bending modes and one stretching mode.

Results on the anharmonicity of the C-H vibration modes in the VN_3H defect in diamond are reported in Table II. Let us discuss first the *intrinsic* anharmonicity of the modes (i.e. when couplings among modes are neglected). In this case, the VSCF and VCI methods, which only differ in the way couplings among modes are treated, provide the same results. A couple of considerations: i) the intrinsic anharmonicity of the stretching mode is rather large and is here found to decrease the harmonic frequency by 129 cm^{-1}; ii) the intrinsic anharmonicity of the bending modes is relatively small and is found to increase the harmonic value by 15 cm^{-1}. When a *complete* anharmonic treatment is performed (i.e. couplings among modes are considered), the VSCF and VCI methods no longer return the same values, VCI always accounting for more anharmonicity than VSCF, as expected. Some considerations: i) by coupling with the two bending modes, the stretching mode is found to further decrease its frequency ω_s by 15 (VSCF) and 28 cm^{-1} (VCI) with respect to the intrinsic anharmonic value; ii) the best VCI computed value for the anharmonic stretching frequency is found to be 3094 cm^{-1}, only 13 cm^{-1} from the experimental value of 3107 cm^{-1}; iii) the coupling with the stretching mode is strongly affecting the anharmonic frequency of the two bending modes ω_b as it is reduced by 30 (VSCF) and 34 cm^{-1} (VCI), which

TABLE II. Anharmonicity of the C-H stretching ω_s and bending ω_b vibration frequencies (all data in cm^{-1}) for the VN_3H defect in diamond. The *intrinsic* anharmonic values refer to a calculation where the couplings among different modes are neglected. The *complete* anharmonic values refer to a calculation where the couplings among the three C-H modes (two degenerate bending and one stretching) are accounted for. The difference Δ between the anharmonic and the harmonic values is given. Experimental values are also reported.[3,4]

	Harmonic	Anharmonic				Exp.
		Intrinsic		Complete		
		VSCF	VCI	VSCF	VCI	
ω_s	3251	3122	3122	3107	3094	3107
Δ		-129	-129	-144	-157	
ω_b	1461	1476	1476	1446	1442	1405
Δ		+15	+15	-15	-19	

results in an anharmonic value for ω_b that is smaller than the harmonic value by 19 cm^{-1} in our best VCI calculation, thus reducing the discrepancy with respect to the experimental value of 1405 cm^{-1}. We are unable to estimate which fraction of the residual difference between simulation and experiment (37 cm^{-1} for VCI) is due to the coupling between the bending modes and other modes of the system, not taken into account here for computational reasons (a full anharmonic treatment of all the 192 normal modes is at the moment out of reach).

As a final word of caution, let us discuss possible "lucky" cancellations of errors in the description of vibrational spectral features of defects in diamond. We have computed harmonic frequencies with the LDA and PBE functionals, for comparison with previous calculations.[12] The harmonic frequency for the C-H stretching is of 3010 cm^{-1} with LDA and of 3096 cm^{-1} with PBE, the latter harmonic value being rather close to the experimental value. However, a rigorous anharmonic treatment would reduce this value by about 150 cm^{-1}. It follows that comparing LDA and GGA harmonic frequencies directly with experiment might result in a spurious agreement due to the "lucky" cancellation of two errors: the poor quality of pure DFT functionals for describing C-H features (the self-interaction error being obviously rather large in this case), and the lack of an explicit anharmonic treatment.

IV. CONCLUSIONS

The structural, electronic, energetic and vibrational spectroscopic features of the VN_3H point-defect in diamond have been characterized by means of accurate quantum-mechanical calculations. Hybrid functionals of the DFT have been adopted, which correct to a large extent for the self-interaction error of pure DFT formulations.

The ground-state of the system is characterized by a closed-shell electronic configuration, with no additional bands within the band-gap of pristine diamond. The H atom, oriented towards the center of the carbon vacancy, strongly interacts with the lone-pair electrons of the three neighboring nitrogen atoms. As a result of the repulsive/polarizing interaction with the N lone-pair electrons, the C-H bond is shorter than it would be in a less constrained case (the isobutane molecule has been used for comparison), and more ionic (with Mulliken net charges of 0.30 and -0.18 $|e|$ for H and C, respectively).

A thorough analysis of the IR and Raman spectroscopic fingerprint of the defect has been reported by means of simulations of peak positions, IR intensities, and Raman intensities. The most peculiar vibrational spectroscopic features are identified in two intense peaks in the IR spectrum that correspond to the C-H stretching and bending motions.

The anharmonicity of these modes has been investigated for the first time by means of VSCF and VCI techniques implemented in a developmental version of the CRYSTAL program. Upon anharmonic correction, the C-H stretching red-shifts by 157 cm^{-1} to the value of 3094 cm^{-1}, at only 13 cm^{-1} from the experimental value of 1307 cm^{-1}. The attribution of this observed spectral feature to the C-H stretching of the VN_3H defect can thus be confirmed. Work is currently in progress to simulate the anharmonic vibration properties of other H-containing defects in diamond in order to check whether they can produce signals in the same spectral region. As per the C-H bending mode, the coupling with the stretching is documented to be essential in order to account for its anharmonic nature.

ACKNOWLEDGMENTS

Prof. Michel Rérat and Dr. Matteo Ferrabone are gratefully acknowledged for their help in the development of the anharmonic methodologies here adopted.

[1] W. G. S and A. T. Collins, J. Phys. Chem. Solids **44**, 471 (1983).
[2] T. Hainschwang, F. Notari, E. Fritsch, and L. Massi, Diamond Relat. Mater. **15**, 1555 (2006).
[3] J. P. Goss, R. Jones, M. I. Heggie, C. P. Ewels, P. R. Briddon, and S. Öberg, Phys. Rev. B **65**, 115207 (2002).
[4] E. Fritsch, T. Hainschwang, L. Massi, and B. Rondeau, New Diamond Frontier Carbon Technol. **17**, 63 (2007).
[5] J. J. Charette, Physica **25**, 1303 (1959).
[6] J. J. Charette, Physica **27**, 1061 (1961).
[7] C. E. Melton, A. A. Giardini, and C. A. Salotti, *Observation of Nitrogen, Water, Carbon-Dioxide, Methane and Argon as Impurities in Natural Diamonds* (1972).
[8] R. M. Chrenko, R. S. McDonald, and K. A. Darrow, Nature **213**, 474 (1967).
[9] J. P. Goss, R. Jones, M. I. Heggie, C. P. Ewels, P. R. Briddon, and S. Öberg, Phys. Status Solidi A **186**, 283 (2001).
[10] P. Briddon, R. Jones, and G. M. S. Lister, J. Phys. C: Solid State Phys. **21**, L1027 (1988).

[11] C. V. Peaker, J. P. Goss, P. Briddon, A. Horsfall, and M. Rayson, Phys. Status Solidi A **212**, 2431 (2015).
[12] J. P. Goss, P. R. Briddon, V. Hill, R. Jones, and M. J. Rayson, J. Phys. Condens. Matter **26**, 145801 (2014).
[13] S. Kümmel and L. Kronik, Rev. Mod. Phys. **80**, 3 (2008).
[14] F. Corà, M. Alfredsson, G. Mallia, D. S. Middlemiss, W. C. Mackrodt, R. Dovesi, and R. Orlando, *The Performance of Hybrid Density Functionals in Solid State Chemistry* (Springer Berlin Heidelberg, Berlin, Heidelberg, 2004), pp. 171–232.
[15] F. Corá, Mol. Phys. **103**, 2483 (2005).
[16] J. M. Crowley, J. Tahir-Kheli, and W. A. Goddard, J. Phys. Chem. Lett. **7**, 1198 (2016).
[17] R. Wahl, D. Vogtenhuber, and G. Kresse, Phys. Rev. B **78**, 104116 (2008).
[18] M. D. L. Pierre, R. Demichelis, and R. Dovesi, *Vibrational Spectroscopy of Minerals Through Ab Initio Methods* (John Wiley & Sons, Ltd, 2016), pp. 341–374.
[19] L. Maschio, B. Kirtman, R. Orlando, and M. Rérat, J. Chem. Phys. **137**, 204113 (pages 11) (2012).
[20] L. Maschio, B. Kirtman, M. Rérat, R. Orlando, and R. Dovesi, J. Chem. Phys. **139**, 167101 (2013).
[21] L. Maschio, B. Kirtman, M. Rérat, R. Orlando, and R. Dovesi, J. Chem. Phys. **139**, 164101 (2013).
[22] L. Maschio, B. Kirtman, M. Rérat, R. Orlando, and R. Dovesi, J. Chem. Phys. **139**, 164102 (2013).
[23] J. Baima, A. Zelferino, P. Olivero, A. Erba, and R. Dovesi, Phys. Chem. Chem. Phys. **18**, 1961 (2016).
[24] S. Salustro, A. Erba, C. Zicovich-Wilson, Y. Noël, L. Maschio, and R. Dovesi, Phys. Chem. Chem. Phys. **18**, 21288 (2016).
[25] S. Salustro, Y. Nöel, C. M. Zicovich-Wilson, P. Olivero, and R. Dovesi, J. Chem. Phys. **145**, 184701 (2016).
[26] S. Salustro, A. Ferrari, R. Orlando, and R. Dovesi, Theor. Chem. Acc. **135** (2016).
[27] S. Salustro, G. Sansone, C. M. Zicovich-Wilson, Y. Noël, L. Maschio, and R. Dovesi, Phys. Chem. Chem. Phys. **accepted** (2017).
[28] Graphical animations of the vibration modes of the VN_3H defect in diamond are available at: http://www.pmmp.jussieu.fr/yves/Jmolvib/?name=freq_128_H.xyz&spt=freq_128_H.spt .
[29] R. Dovesi, R. Orlando, A. Erba, C. M. Zicovich-Wilson, B. Civalleri, S. Casassa, L. Maschio, M. Ferrabone, M. D. L. Pierre, P. D'Arco, et al., Int. J. Quantum Chem. **114**, 1287 (2014).
[30] A. D. Becke, J. Chem. Phys. **98**, 5648 (1993).
[31] C. Lee, W. Yang, and R. G. Parr, Phys. Rev. B **37**, 785 (1988).
[32] W. J. Hehre, R. Ditchfield, and J. A. Pople, J. Chem. Phys. **56**, 2257 (1972).
[33] P. Dirac, Proc. R. Soc. A **126**, 360 (1930).
[34] J. P. Perdew, K. Burke, and M. Ernzerhof, Phys. Rev. Lett. **77**, 3865 (1996).
[35] C. Adamo and V. Barone, Chem. Phys. Lett. **298**, 113 (1998).
[36] A. V. Krukau, O. A. Vydrov, A. F. Izmaylov, and G. E. Scuseria, J. Chem. Phys. **125**, 224106 (2006).
[37] R. Dovesi, V. R. Saunders, C. Roetti, R. Orlando, C. M. Zicovich-Wilson, F. Pascale, B. Civalleri, K. Doll, N. M. Harrison, I. J. Bush, et al., *CRYSTAL 2014 User's Manual* (University of Torino, Torino, 2013).
[38] F. Pascale, C. M. Zicovich-Wilson, F. L. Gejo, B. Civalleri, R. Orlando, and R. Dovesi, J. Comput. Chem. **25**, 888 (2004).
[39] C. M. Zicovich-Wilson, F. Pascale, C. Roetti, V. R. Saunders, R. Orlando, and R. Dovesi, J. Comput. Chem. **25**, 1873 (2004).
[40] A. Erba, M. Ferrabone, R. Orlando, and R. Dovesi, J. Comput. Chem. **34**, 346 (2013).
[41] C. Carteret, M. De La Pierre, M. Dossot, F. Pascale, A. Erba, and R. Dovesi, J. Chem. Phys. **138**, 014201 (2013).
[42] J. Baima, M. Ferrabone, R. Orlando, A. Erba, and R. Dovesi, Phys. Chem. Minerals **43**, 137 (2016).
[43] F. Pascale, C. M. Zicovich-Wilson, R. Orlando, C. Roetti, P. Ugliengo, and R. Dovesi, J. Phys. Chem. B **109**, 6146 (2005).
[44] F. Pascale, P. Ugliengo, B. Civalleri, R. Orlando, P. DArco, and R. Dovesi, J. Chem. Phys. **117**, 5337 (2002).
[45] G. M. Barrow, *Introduction to molecular spectroscopy* (McGraw-Hill, New York, 1962).
[46] B. A. Hess, L. J. Schaad, P. Carsky, and R. Zahradnik, Chem. Rev **86**, 709 (1986).
[47] D. A. McQuarrie and J. D. Simon, *Physical Chemistry. A Molecular Approach* (University Science Books, Sausalito, CA, 1977).
[48] M. Mérawa, P. Labeguerie, P. Ugliengo, K. Doll, and R. Dovesi, Chem. Phys. Lett. **387**, 453 (2004).
[49] P. Ugliengo, F.Pascale, M. Merawa, P. Labéguerie, S. Tosoni, and R. Dovesi, J. Phys. Chem. B **108**, 13632 (2004).
[50] R. Orlando, F. J. Torres, F. Pascale, P. Ugliengo, C. M. Zicovich-Wilson, and R. Dovesi, J. Phys. Chem. B **110**, 692 (2006).
[51] F. Pascale, S. Tosoni, C. M. Zicovich-Wilson, P. Ugliengo, R. Orlando, and R. Dovesi, Chem. Phys. Lett. **396**, 308 (2004).
[52] S. Tosoni, F. Pascale, P. Ugliengo, R. Orlando, V. R. Saunders, and R. Dovesi, Molecular Physics **103**, 2549 (2005).
[53] R. Demichelis, Y. Noël, B. Civalleri, C. Roetti, M. Ferrero, and R. Dovesi, J. Phys. Chem. B **111**, 9337 (2007).
[54] C. Lin, A. Gilbert, and P. Gill, Theor. Chem. Acc. **120**, 23 (2008).
[55] J. M. Bowman, J. Chem. Phys. **68**, 608 (1978).
[56] J. M. Bowman, Acc. Chem. Res. **19**, 202 (1986).
[57] R. B. Gerber and M. A. Ratner, Chem. Phys. Lett. **68**, 195 (1979).
[58] R. B. Gerber and M. A. Ratner, Adv. Chem. Phys. **70**, 97 (1988).
[59] K. M. C. J. M. Bowman and F. Tobin, J. Phys. Chem. **83**, 905 (1979).
[60] K. M. Christoffel and J. M. Bowman, Chem. Phys. Lett. **85**, 220 (1982).
[61] J. M. B. S. Carter and N. C. Handy, **100**, 191 (1998).
[62] G. S. Woods and A. T. Collins, J. Phys. C: Solid State Phys. **15**, L949 (1982).
[63] M. Torrent-Sucarrat, J. M. Anglada, and J. M. Luis, Phys. Chem. Chem. Phys. **11**, 6377 (2009).
[64] M. Biczysko, J. Bloino, I. Carnimeo, P. Panek, and V. Barone, J. Mol. Struct. **1009**, 74 (2012).
[65] J. Bloino, J. Phys. Chem. A **119**, 5269 (2015).
[66] J. L. Duncan, D. C. McKean, I. T. A. Brown, and A. M. Ferguson, J. Chem. Soc., Faraday Trans. 2: Molec. Chem. Phys. **84**, 1423 (1988).
[67] M. L. Myrick, A. E. Greer, A. A. Nieuwland, R. J. Priore, J. Scaffidi, D. Andreatta, and P. Colavita, J. Chem. Educ. **85**, 1276 (2008).